A boundary layer inspection on a wing profile through high resolution thermography and numerical methods

M. MALERBA, M. ARGENTO, A. SALVIUOLO, G.L. ROSSI
Dipartimento di Ingegneria Industriale
Università degli Studi di Perugia
Via G. Duranti, 67 – 06125 Perugia (PG)
ITALY
malerba@unipg.it m.argento@unipg.it salviuolo@mec.dii.unipg.it gianluca@unipg.it

Abstract: - In fluid-dynamic phenomena the boundary layer plays a fundamental role. It also affects the drag and lift force of a body immersed in a fluid. Reynolds analogy introduces the possibility to correlate fluidynamic to thermal field. By using high sensitivity thermographic systems, temperature pattern on the surface of solid bodies immersed into a fluid can be analysed. Temperature distribution depends on many combined effects, such as: conversion of kinetic energy of the flow into thermal energy, flow temperature variation in time and space, convection heat transfer phenomena between flow and body, conduction phenomena inside the body, and radiation heath exchange.
A numerical approach is used to compare results of the proposed procedure. A transient simulation with increasing inlet fluid temperature is carried out to evaluate the thermal exchange between the airstream and the body. The effect of the different thermal exchange due to the local flow peculiarity is modelled.

Key-Words: Boundary layer, Infrared thermography, Subsonic flow, Passive technique, Wing profile, CFD

Nomenclature

k	Thermal conductivity
Nu	Nusselt number
Nu_x	Local Nusselt number
Re	Reynolds number
Re_x	Local Reynolds number
Pr	Prandl number
C_f	Surface shear stress coefficient
C_{fx}	Local surface shear stress coefficient
ν	Kinematic viscosity
h_x	Convective coefficient
Φ	Heat flux exchange
T_∞	Temperature of the fluid
T	Temperature of the body surface
ρ	Density
$\Phi_{cond.lat.}$	Thermic stream due to lateral conduction
Φ_j	Thermic stream due to Joule's effect
Φ_{rad}	Thermic stream due to radiation effect
e	Thickness

1 Introduction

In all aerodynamic aspects, the knowledge of boundary layer pattern plays a fundamental role on the analysis of fluid dynamic phenomena and on interaction between solid bodies and surrounding fluid flow. Systems based on high resolution thermographic visualization seem to be very interesting measurement techniques to monitoring it. These systems detect temperature distribution of a body surface. Measurement principles adopted are based on the heat exchange that take place between a solid body and the surrounding fluid flow. In this situation, temperature pattern is due to three different phenomena: thermodynamic effects of fluid flow temperature modify due to the friction, heat transfer phenomena by convection between flow and body and conduction phenomena inside the body. If we neglect conduction phenomenon, the energy associated with convection between body and fluid, can be described by [1]:

$$\Phi = h_x(T - T_\infty) \qquad (1)$$

where heat transfer coefficient h_x change both if the flow is laminar or turbulent [8-10].
If the body is moving across a fluid, a correlation between thermographic and fluid-dynamic pattern can be done. A well known hypothesis that permits this correlation is Reynold's analogy, expressed by the following relation [2]:

$$\frac{Nu_x}{Re_x \cdot Pr} = \frac{C_{fx}}{2} \qquad (2)$$

In particular, as described in [3], assuming Pr = 1, the previous equation gives rise to the following linear relationship between convective and skin friction coefficients.

$$C_{fx} = 2 \cdot \frac{\nu \cdot h_x}{c \cdot k} \qquad (3)$$

This equation correlates heat exchange coefficient h_x and local surface shear stress coefficient C_{fx}, so it is possible to carry out information about boundary layer pattern [4]. The visualized temperature distribution (figure 1) is correlated with property of the external flow and the ones of the body. If the body is cooler than air, it will be characterized by an increasing of temperature due to tangential conduction, followed by a first decrement in the flow acceleration zones. After this, temperature starts to decrease quickly due to the change of h_x and then it starts to rise. The area of temperature trend inversion is usually characterized by a fluid-dynamics transition (laminar to turbulent) or aerodynamic bubble. The maximum gradient of temperature is generally located in a very small area close to the antinode of the profile. Experimental tests have be done to visualize this pattern using different samples, materials and measurement chains. Only the more representative are illustrated in this work [5]. The goal is to search for a numerical comparison to have more information about this phenomenon.
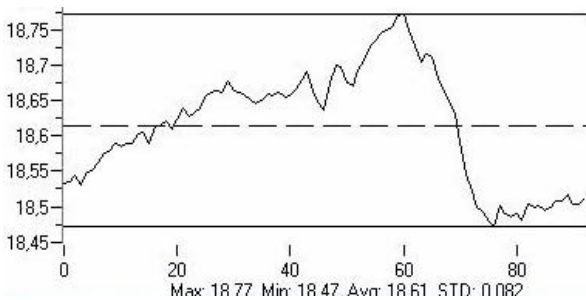

Fig. 1: Classic temperature distribution on a wing: the x-axis is the coordinate along the chord of the wing, the y-axis is the measured temperature.

2   Theoretical issue

Reynold's analogy is not sufficient for an exhaustive analysis, it must be associated to the internal energy of the fluid flow that is strictly correlated with Mach number. Generally working with high Mach numbers (i.e. transonic flow or more) a direct reading of energy can be done [10]. This energy in slow subsonic flows (i.e. very low

Mach number) is not sufficient to produce a remarkable heat gradient on the body surface. Frequently this problem can be resolved in two different way: the first one, called "*active technique*", needs to heat the body surface artificially, the other ("*passive technique*") wants the fluid flow heated. Passive technique is less intrusive for the physical phenomenon.

The most used method to monitor motion field by thermographic measurement is an active – stationary called *heated-thin-foil technique* [6-7-8-9]. It consists of heating the observed body by metallic sheets, like copper or similar, or by printed circuit boards. By monitoring temperature and knowing thermal flow produced by Joule's effect, it is possible to find thermal convection coefficient between body and fluid using the energy balance expression:

$$h = \frac{\left(\Phi_j - \Phi_{cond.lat} - \Phi_{rad} \right)}{\left(T - T_\infty \right)} \qquad (4)$$

An alternative way to proceed is to use transient flow condition and passive set-up. It is represented by the *thin skin technique*. In this case the body is considered with reduced thermal capacity and resistance. Under determined assumption it is possible to suppose an instantaneous heat transfer inside the body until equilibrium and consequently internal conduction can be neglected.

Referring to the general equation of heat conduction without thermal source, this case is represented by:

$$\Phi = c \cdot \rho \cdot e \cdot \frac{\partial T}{\partial t} \qquad (5)$$

As a result of this relation, informations about convection coefficient can be obtained just monitoring the temporal development of superficial temperature [12]:

$$h = \frac{\left(c \cdot \rho \cdot e \cdot \frac{\partial T}{\partial t} \right)}{\left(T_\infty - T \right)} \qquad (6)$$

In another way it is possible to admit hypothesis of *semi-infinite body* in which is theoretically expectable the thermal pattern due to conduction. Body temperature is representable by the following relation [13]:

$$T = \frac{1}{2 \cdot \sqrt{\pi \cdot a \cdot t}} \cdot \int_{-\infty}^{\infty} f(x') e^{-\frac{(x-x^*)^2}{4 \cdot a \cdot t}} \cdot dx' \qquad (7)$$

The last two hypothesis, concerning with flow heating, enforce a passive technique work.

3 Experimental test

Experimental tests are used to investigate in qualitative way boundary layer pattern of an airfoil. The goal is to connect it to thermal maps in slow subsonic flow condition and to compare direct vision with passive technique. Two type of tests have been conducted. The first one adopts an open circuit wind tunnel where temperature pattern can be considered constant. The second set uses a closed circuit wind tunnel where passive method is adopted using the own heating of the wind tunnel. Thermographic system used is an high sensitivity CCD thermocamera, manufactured by Stress Photonics, the Deltatherm 1560 system.

3.1 Open circuit wind tunnel

An aluminium wing profile (figure 2) with length of 153 mm and chord of 100 mm was tested in a slow subsonic wind tunnel with a test section of 400*400 mm (figure 3). Function typology is by aspiration. Aluminium is choose for its internal high conductivity. Temperature and wind speed were monitored by a thermal resistor and a Pitot's tube positioned inside the tunnel. Measured temperature gradient was minor than 0,01 K, therefore temperature is considered as a constant for the specific issue.

Fig. 2: Aluminium wing profile

A first test was done covering the profile with black paint to avoid reflection effects and different emissivity values effects on its surface. The wing profile was fixed by one end using a 0 degrees angle of attach on the test section of the wind tunnel.
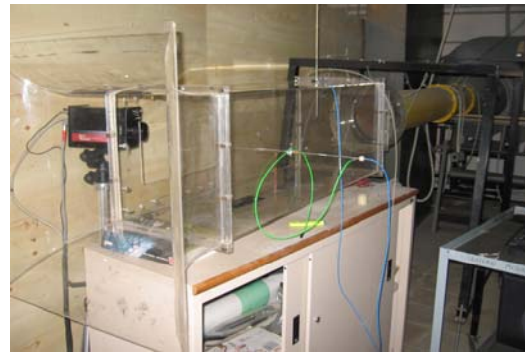
Fig. 3: Open circuit wind tunnel

Acquired thermographic images show that convection thermal exchange between flow and body propagate very quickly. Diagrams in each thermographic image describe temperature pattern along the investigation line traced over the profile (the arrow in the figure). Temperature is shown using Celsius scale. Due to aluminium high conductivity inside the body the temperature pattern shows only a temperature increment with thickness profile decrement (figure 4).
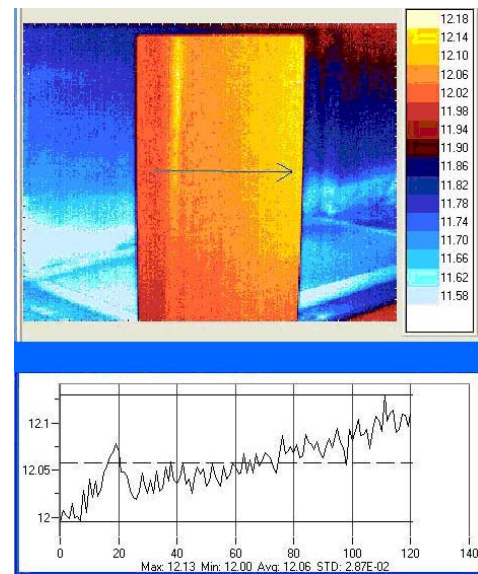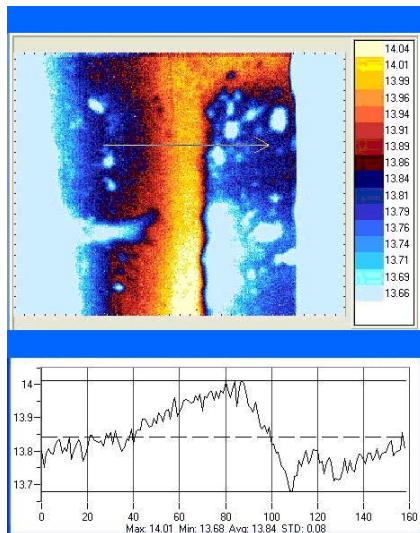

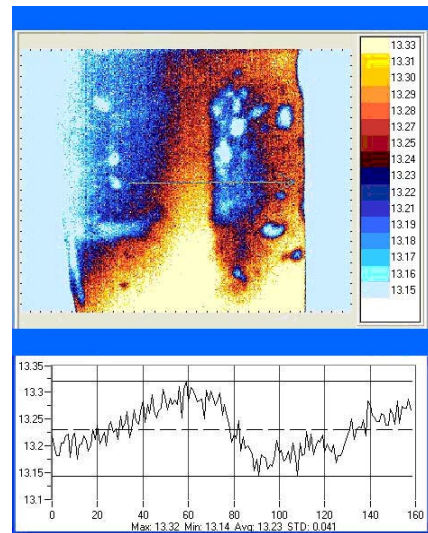Fig.4: Temperature distribution for aluminium airfoil

To take out high conductivity effects, the profile was covered with a film of Mylar® with a thickness of 36 μm. Mylar® is an insulation, strong and durable polyester film. Its thermal properties are summarized in the table 1.
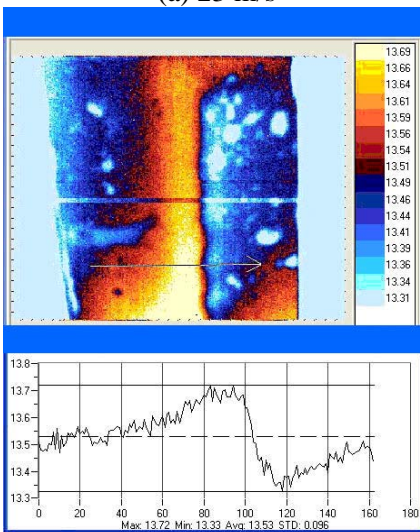
Table 1: Typical Value of Mylar® film

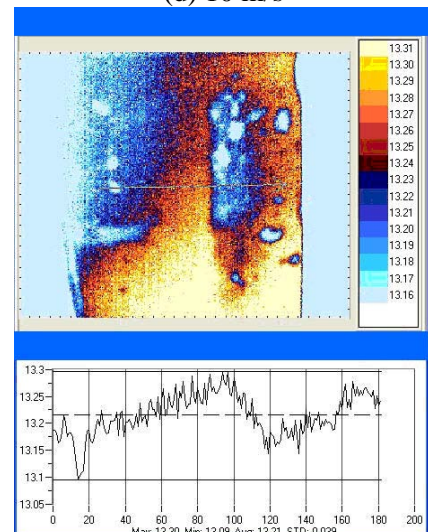| Property	Typical Value	Unit
Specific Heat	1172	J/kg *K
Thermal Conductivity	1.5 E-04	W/mm* K

(a) 23 m/s

(b) 22 m/s
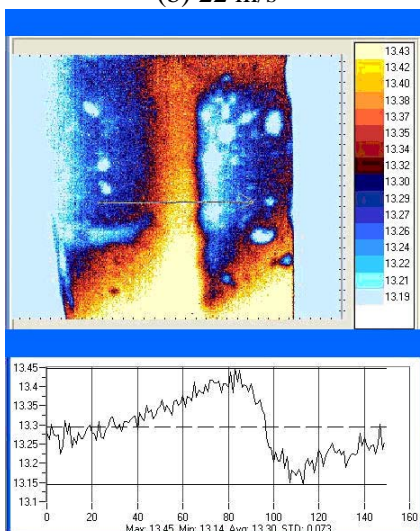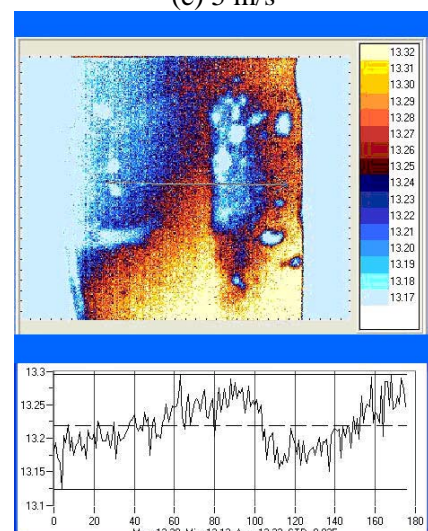

(c) 19 m/s

(d) 10 m/s

(e) 5 m/s

(f) 2 m/s

Fig. 5 (a,b,c,d,e,f): Temperature distribution for aluminium airfoil black painted and Mylar® 36 μm covered.

To avoid reflection effects, it was also covered by a black film, with an high emissivity coefficient.

Tests were accomplished modifying flow velocity that presented following values: 23 m/s, 22 m/s, 19 m/s, 10 m/s, 5 m/s and about 2 m/s (Re between $1*10e5 \div 1*10e6$).

The images in fig. 5 show temperature pattern on the surface of wing profile at different wind speed.

It can be observed that for 23, 22 and 19 m/s velocity temperature pattern is the typical previously described: an increment to the transition zone followed by a decrement.

For lower velocity after the decrease due to the aerodynamic bubble there is a new temperature increase, less marked when the velocity reduces.

For the first three images there is a clearly transition area, while for the last three phenomenon it is less marked (i.e. there is not a sufficient energy exchange).

A second session of tests was done by covering the wing profile with a 12 μm thickness film of Mylar®. Boundary layer pattern was the same of last test. The following image (fig. 6) is obtained using a flow velocity of 23 m/s. It shows that temperature pattern is the typical previously described: temperature raise and the decrease to the transition zone. In this case image has been scaled by subtraction to initial condition. Temperature range is 10^{-03} degree. Figures 7 and 8 are scaled in the same way. Tests were realized with speed value of the other session.
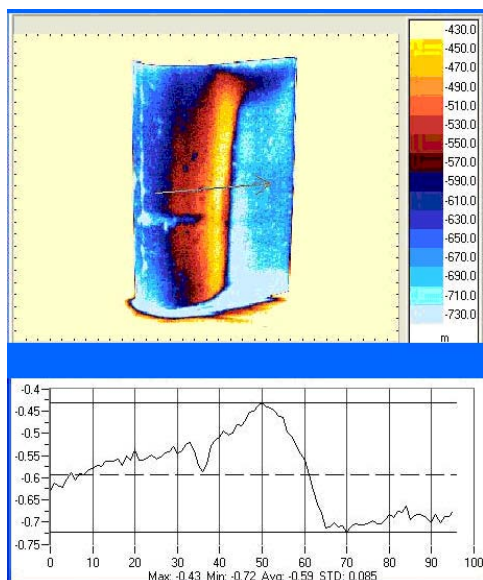

Fig. 6: Temperature distribution for aluminium airfoil black painted and Mylar® 12 μm covered in open circuit wind tunnel

To confirm results another set of tests was accomplished using an angle of attach of 7,5

degrees clockwise. Acquired thermographic images (figure 7) show a boundary layer pattern shifted compared to the one obtained for 0 degree angle of incidence.

Rotating of 7,5 degrees counter clockwise the profile, acquired thermographic images (figure 8) show a different boundary layer pattern, in fact there isn't temperature gradient.
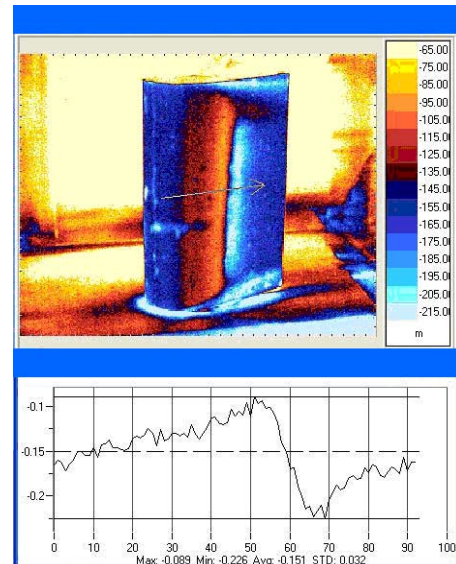

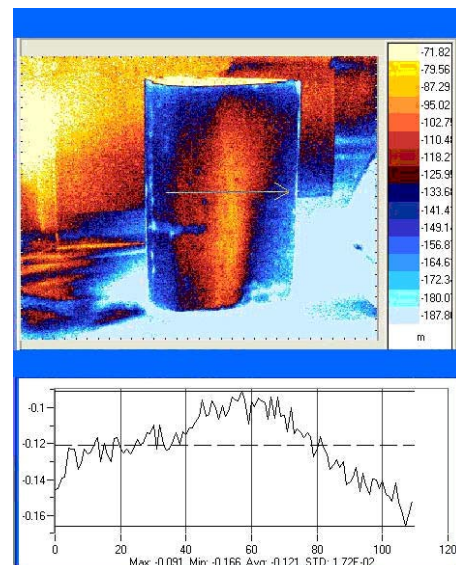Fig. 7: Airfoil with incidence of 7,5° clockwise

Fig. 8: Airfoil with incidence of -7,5° clockwise

3.2 Closed circuit wind tunnel

To validate and confirm the techniques, airfoil was tested also in a different subsonic wind tunnel with a test section of 2200x2200mm and recirculating flow.
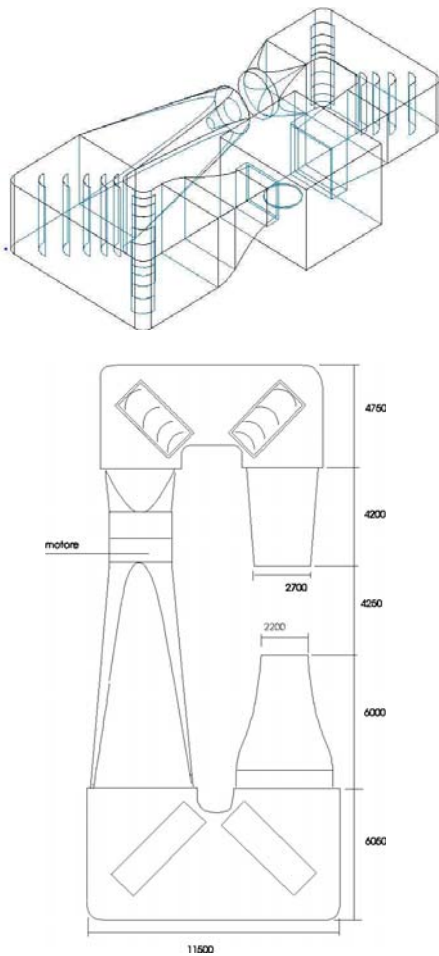
Fig. 9: 3d visualization and layout plan of closed circuit wind tunnel

During the wind tunnel run, air temperature increases by friction due the interaction with the honey-comb in the tunnel.
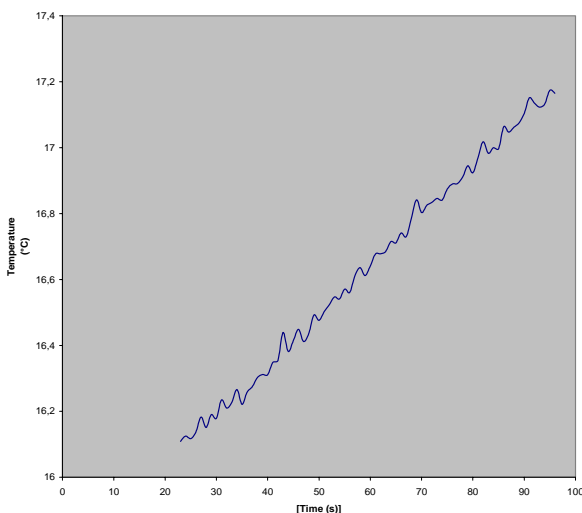

Fig. 10: Measured air temperature pattern in closed circuit wind tunnel during a standard test

Tests were accomplished by using passive technique. Flow velocity during the test was fixed at the value of 42 m/s.

Also in this case wing profile was covered by a film of Mylar® with a thickness of 12 μm and a black film on it. It was positioned in the wind tunnel using a 0 degrees angle of attack.
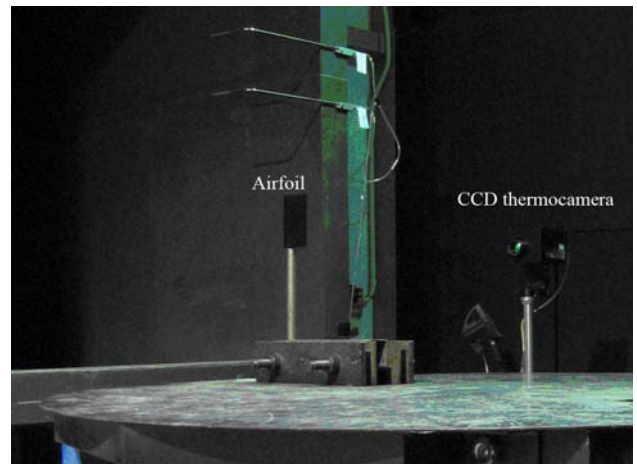
Fig. 11: Airfoil positioned in closed circuit wind tunnel

In this case airfoil is colder than fluid so that when fluid arrives to the leading edge of the body starts to warm for tangential conduction phenomena [9]. After fluid detaches, superficial temperature became constant.

The gradient of temperature is the one that appears when boundary layer detaches. In this case it is reversed if compared with the previous because the body was warmed by the flow (figure 12).
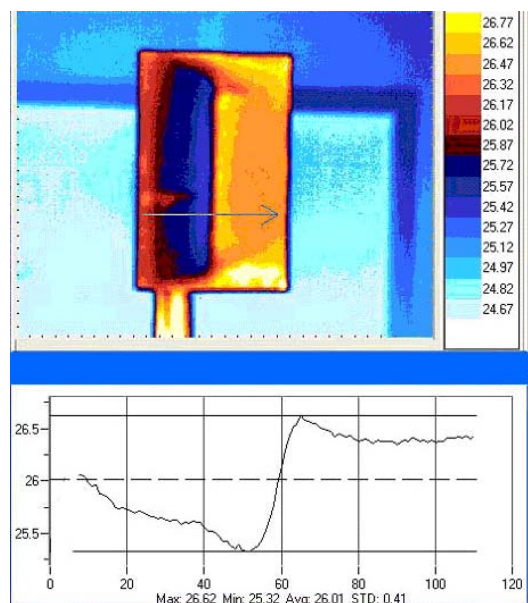

Fig.12: Temperature distribution for airfoil tested in closed circuit wind tunnel

In a second test the angle of attach was changed rotating the airfoil of 7.5 degrees clockwise. Results are similar to the last case (Figure 13).
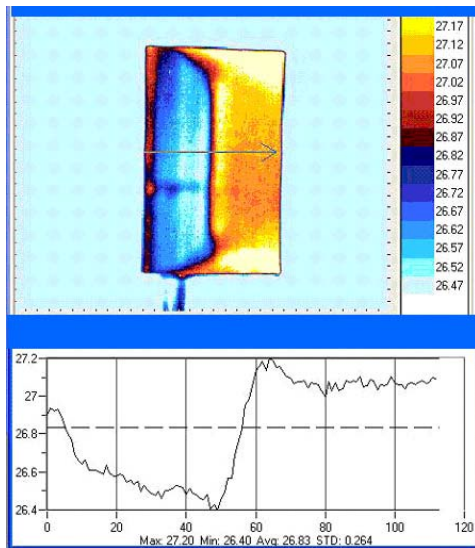

Fig.13: Temperature distribution for airfoil tested in closed circuit wind tunnel with incidence of 7,5° clockwise

4 Numerical approach

If the results obtained with the calculus are close to the experimental data, it's possible to validate them. After this step it is possible to use results to explore not only the temperature distribution over the surface of the body but also the flow field surrounding the wing.

Different analytical models were used to determine the best solution both in a steady and in an unsteady state.

A first set of analyses were accomplished using a 2d model to better understand the behavior of the system and to set up the numerical parameters of the simulation. Then a 3d model was implemented.

Furthermore, a very fine grid must be used for the analysis, the local flow separation phenomenon involves the heat exchange behavior. .
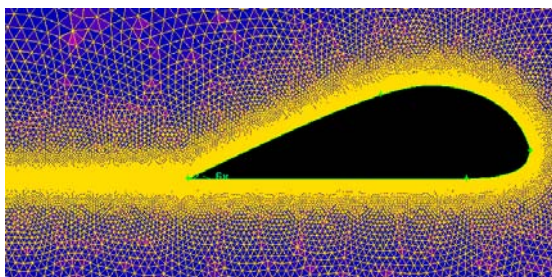

Fig. 14: Discretization of the 3d model over a middle plane of the wing

Figure 14 shows the mesh adopted with a thin boundary layer and a finest zone to resolve the wake. It was obtained extruding the planar grid of the 2d model

4.1 The model adopted

The main approaches selected to simulate the process are two: the first and less costly method is based on the RANS model; then a LES model was used to examine the small scale phenomena.

The first set of the analyses is executed using the k-ε realizable model with wall function and enabling the viscous heating option. The inlet and the outlet boundary conditions are imposed using the experimental conditions. Velocity, temperature, pressure and turbulence (the length scale has the magnitude of the honeycomb cells) are the same of the test section of the wind tunnel.

The thermal equilibrium was reached assigning an adiabatic condition to the surface of the body, *i.e.* neglecting temperature sources. The physical properties of the Mylar are assigned to the wall of the wing.

The low Mach number and the very small temperature gradient justify an incompressible fluid formulation.

The second set of the analyses adopt the LES model. A time step of 5e-05 sec. was used and the results are observed for a period of 0.02 seconds.

A sub-domain surrounding the wing was extracted from the first one used in the steady state calculation. The results obtained using the RANS model were used as boundary condition for the LES simulation. In this way it's possible to adopt a finest grid than the first one. This strategy is an usual way to resolve the smaller turbulent scales when a 3d LES model is used [14].
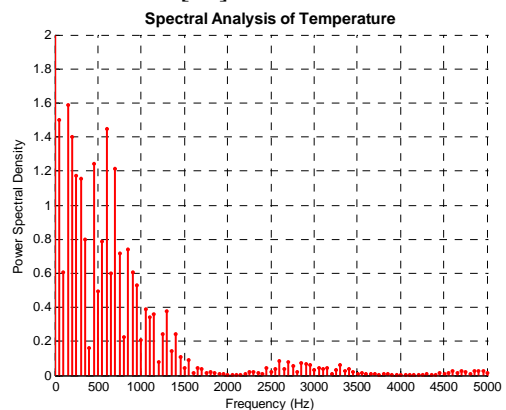

Fig. 15: Temperature Spectral Density at a node

The spectrum of the unsteady behaviour of the flow is shown in figures 15 and 16. The main events

occur at a frequency from 0 to 2000 Hz, so the time step used can describe the flow.
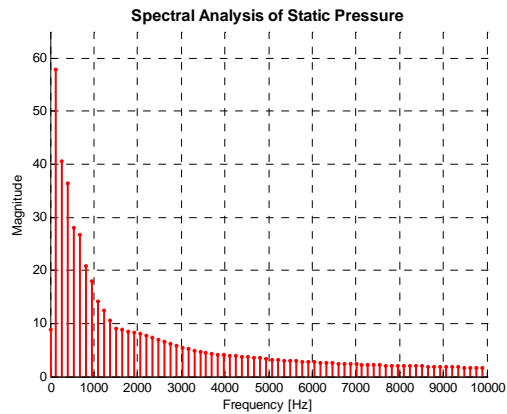

Fig. 16: Static Pressure Spectral Density at a node

4.2 The results

All the analyses are performed using a commercial CFD package.

The results are evaluated with the aid of the flow field contour map and by plotting the temperature distribution along the upper side of the wing profile over its middle plane.

The RANS method calculation is presented in figure 17. The diagram in figure 18 shows a positive gradient of temperature starting from the leading edge to the "hump" according with the experimental data. Then the temperature decreases up to the trailing edge of the wing. The two equation based on models, such as k-ε, can't resolve completely the flow separation and the transition between laminar and turbulence boundary layer [14, 15].
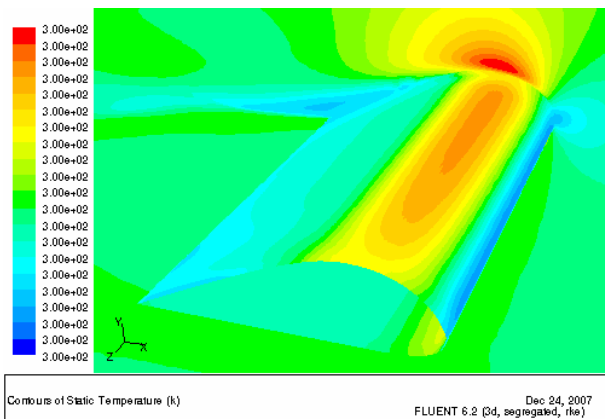

Fig 17: Temperature distribution (3d RANS model)

A modified turbulence viscosity model [15] could be used to overcome this occurrence. This could be

implemented by using the experimental observation and the Reynolds Analogy in order to switch the heat transfer coefficient between a laminar and a turbulent value. An other, but more expensive way to explore the heat exchange is the LES model. The following figures and diagrams show the results obtained for two different time steps.
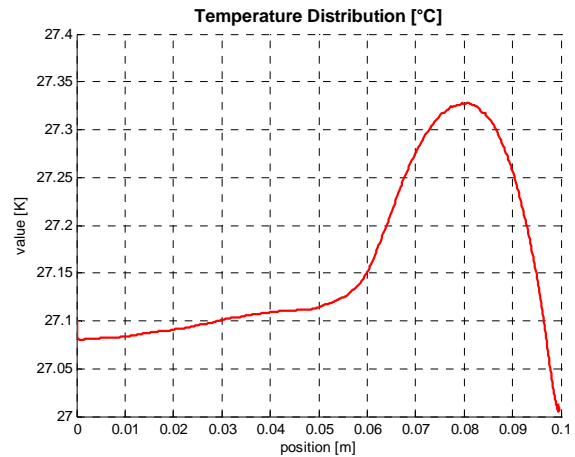

Fig. 18: Temperature distribution along the suction side for the RANS 3d model solution
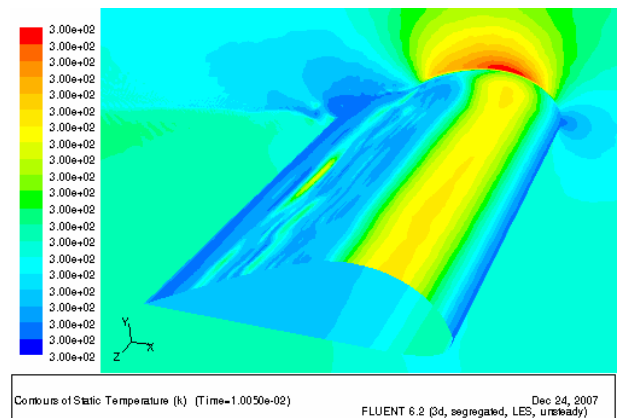

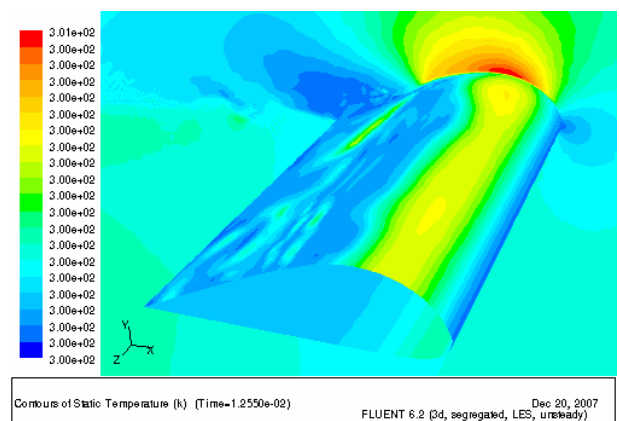Fig. 19: Temperature field at 0.1 sec

Fig. 20: Temperature field at 0.125 sec.

The leading edge temperature distribution is the same as the obtained one using the k-ε model. Afterwards some "picks" of temperature occur close to the zone at a greater vorticity. The turbulent heat exchange is thus greater than in laminar zone. Figure 19 and figure 20 show this occurrence. Velocity vectors at two different time step are shown in figures 21 and 22.
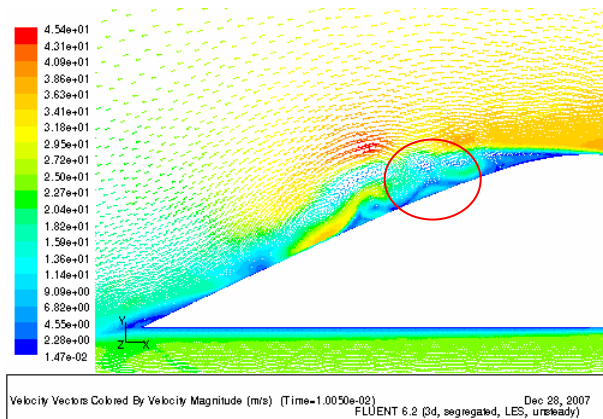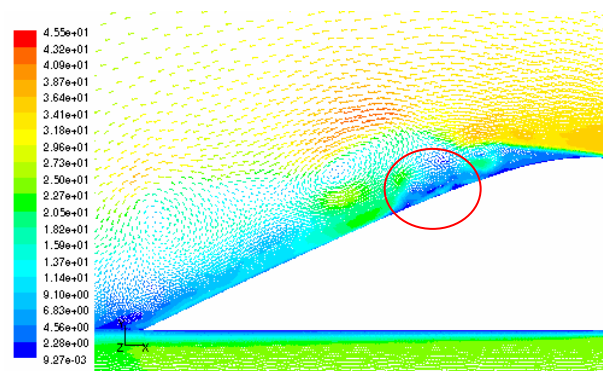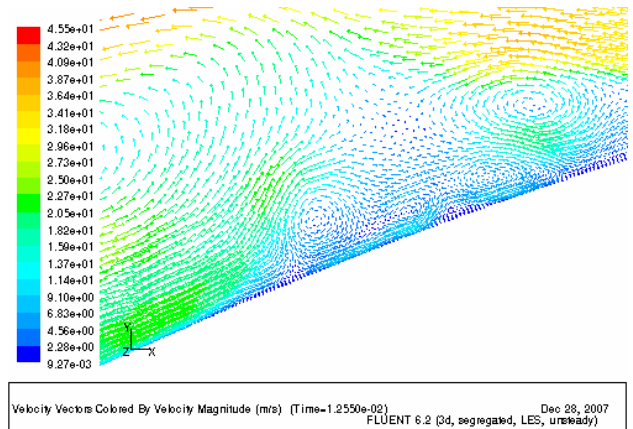

(a)
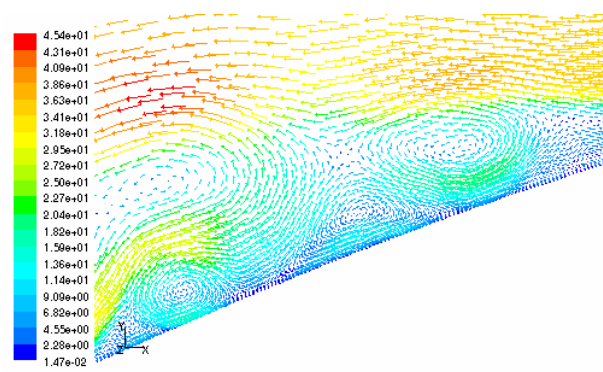
(b)

Fig. 21: a) Velocity vectors at 0.1 sec colored by velocity magnitude, b) detailed view

(a)

(b)

Fig. 22: a) Velocity vectors at 0.125 sec colored by velocity magnitude, b) detailed view

Diagrams in figure 23 and 24 report the temperature variation along the chord at different time steps.
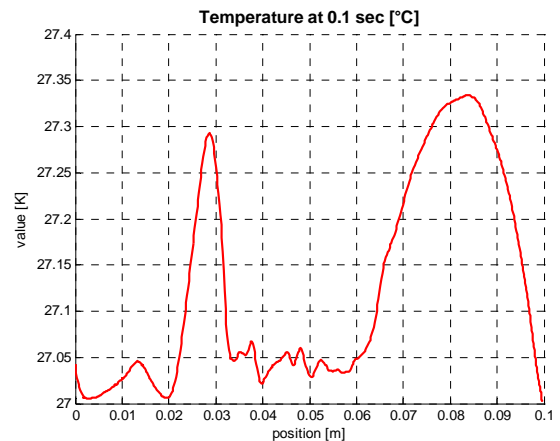

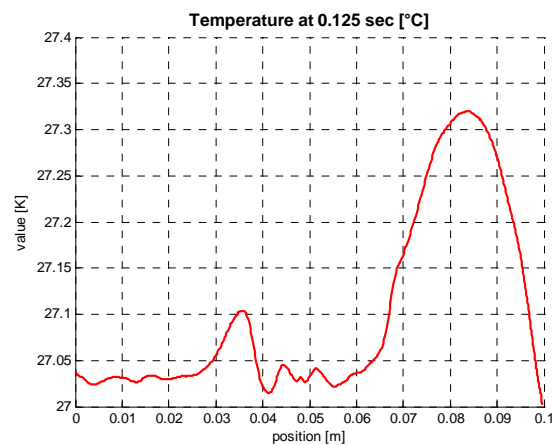
Fig. 23: Temperature distribution at 0.1 sec.

Fig. 24: Temperature distribution at 0.125 sec.

The last consideration can be done with the aid of the medium value obtained averaging all the results. The temperature distribution along the chord of the wing is similar to the other analyses in the zone close to the leading edge. However, moving toward the trailing edge a small increase of temperature occurs (figure 25). This behaviour is more similar to the experimental results obtained.
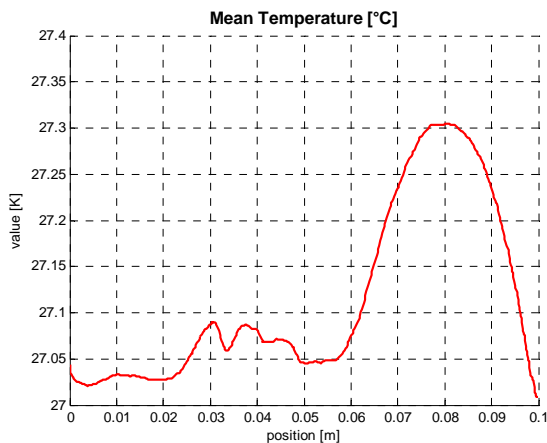

Fig. 25: Averaged temperature along the chord

Inside the wake the mean temperature contours differ from the ones obtained with the RANS method (fig. 26).
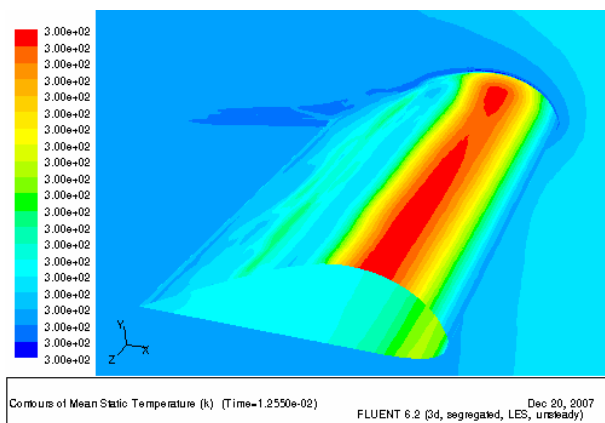

Fig. 26: Contours of Mean Temperature

Finally, both the averaged value and the time dependent solution are related to the total time of observation and to the sampling frequency.

5   Conclusion

Results explained on this paper, demonstrate that the high sensitivity thermographic technique can be used to obtain a fast qualitative evaluation of boundary layer also for low subsonic flow.

The difference between experimental and numerical data can be seen firstly in the slope of the initial ramp starting from the leading edge of the profile. The experimental value rises more slowly than the numerical data. This can be explained considering the one-dimensional thermographic images versus the bi-dimensional distribution of the numerical data. The models adopted show a good accordance with the experimental data in terms of macroscopic behaviour. To understand the small scale and unsteady events the LES approach is more reliable.

References:

[1] E. Gartenberg, A. S. Roberts Jr., Twenty-Five Years of Aerodynamics Research with Infrared Imaging, *Journal of Aircraft*, Vol.29, No2, March-April 1992

[2] F. Kreith, *Principi di Trasmissione del Calore* , Liguori Editore,1988

[3] E. Gartenberg, A. S. Roberts Jr., G. J. McRee, *Infrared Imaging and Tufts Studies of Boundary Layer Flow Regimes on a NACA 0012 Airfoil*, CH2762-3/89/0000-0168, 1989 IEEE.

[4] I. Barducci, *Trasmissione del Calore*, Vol.1, Milano 1991, Editoriale ESA

[5] M. Malerba, A. Salviuolo, G.L. Rossi, Qualitative fluid-dynamic analysis of wing profile by thermographic technique, *XIV A.I.VE.LA National Meeting,* November 2006.

[6] G. M. Carlomagno, L. De Luca, Infrared Thermography for Flow Visualization and Heat Transfer Measurement, *Workshop on: Stato dell'arte del rilevamento con Camere Termiche nella banda 8-14micron,* 1991, pp.191-219

[7] G. M. Carlomagno, G. Cardone, T. Astarita, Wall Heat Transfer in Static and Rotating 180° Turn Channels by Quantitative Infrared Thermography, *Rev. Gen. Therm.*, 37, 1998, pp. 644-652, Elsevier Science, Paris.

[8] G. Cardone, T. Astarita, Thermofluidynamics Analysis of the Flow in a Sharp 180° Turn Channel, *Experimental Thermal and Fluid Science,* 20, 2000, pp. 188-200, Elsevier Science.

[9] T. Astarita, G. Cardone, G. M. Carlomagno, C. Meola, A survey on Infrared Thermography for Convective Heat Transfer Measurement, *Optics & Laser Technology*, 2001, Elsevier Science

[10] J. E. Lamar, Flow Visualization Techniques Used at High Speed by Configuration Aerodynamics Wind-Tunnel-Test Team, *NASA report*, No TM-2001-210848, April 2001

[11] D. L. Balageas, A-M. Bouchardy, Application of Infrared Termography in Fluid Mechanics", Lecture Series on "Measurement Techniques, *Von Karman Institute for Fluid Dynamics*, 1993-05

[12] M. Carbonaro, P. Maggiorana, R. Marsili, An innovative methodology in the characterization of halogen lamp as reference source for Heat Flux Sensors calibration, *Measurement Science and Technologies*, June 02, Institute of Physics Publishing

[13] H. S. Carslaw, J.C. Jaeger, *Conduction of Heat in Solids*, Second Edition, Oxford Science Pubblications,1990

[14] J. H. Fersiger, M. Peric, *Computational Methods for Fluid Dynamics,* Springer, 2002

[15] H.K. Versteeg, W. Malalasekera, *An Introduction to Computational Fluid Dynamics*, Longman, 1995